

## MODAL BASED TANPURA SIMULATION: COMBINING TENSION MODULATION AND DISTRIBUTED BRIDGE INTERACTION

Jamie Bridges, Maarten Van Walstijn

Sonic Arts Research Centre  
 School of Electronics, Electrical Engineering, and Computer Science  
 Queen's University Belfast, UK  
 {jbridges05, m.vanwalstijn}@qub.ac.uk

### ABSTRACT

Techniques for the simulation of the tanpura have advanced significantly in recent years allowing numerically stable inclusion of bridge contact. In this paper tension modulation is added to a tanpura model containing a stiff lossy string, distributed bridge contact and the thread. The model is proven to be unconditionally stable and the numerical solver used has a unique solution as a result of choices made in the discretisation process. Effects due to the distribution of the bridge contact forces by comparison to a single point bridge and of introducing the tension modulation are studied in simulations. This model is intended for use in furthering the understanding of the physics of the tanpura and for informing the development of algorithms for sound synthesis of the tanpura and similar stringed instruments.

### 1. INTRODUCTION

The tanpura is an Indian stringed instrument known for its distinctive droning sound which features a time-dependent formant of frequencies referred to as the "jvari". The generation of the jvari depends heavily on the interaction between the strings and the bridge over which they pass. The jvari also relies strongly on the position of a thread which is placed between each string and the bridge. This changes how much of the string can interact with the bridge and only when placed within a certain range of positions will the tanpura produce the jvari [1]. The sound of the jvari can be altered by moving the thread within the range.

The interaction between barriers and strings is not unique to this instrument; models of the guitar [2], violin [3] and many others have been developed which include this phenomenon. The non-analytic nature of contact forces requires some care to be taken to ensure that any model including them will be stable. Energy methods proved to be an effective way to maintain stability [4, 5, 6] by ensuring that the numerical energy or some analogous quantity is conserved for all time steps when there are no energy losses or gains from external factors. Within the umbrella of energy methods there are differing approaches to creating models; differentiation in time can be carried out with different approximations giving a temporal second order form [7] or a temporal first order form [5]. Models of stringed instruments have made use of finite difference methods [8, 5] as well as modal based methods [9]. The latter allow completely eliminating numerical dispersion by exactly fixing the modal frequencies and damping which removes mode detuning [9]. This is particularly important in the case of the tanpura as the jvari is sensitive to any numerical warping of the partial structure. In addition to unconditional stability it is possible to ensure that the numerical solver has a unique solution [9] which in conjunc-

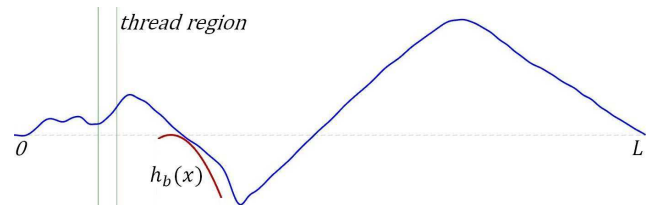


Figure 1: A simplified sketch of the tanpura model with the thread and bridge zoomed in on significantly.

tion with the stability allows the model to be run at standard audio sampling frequencies and maintain global trends.

In this paper tension modulation and a distributed bridge are included in a model of the tanpura. A sketch of the model is shown in Figure 1. Both of these effects have been modelled in musical acoustics before but they have not yet been brought together in a tanpura model. Tension modulation has been recently considered in the modelling of Portuguese twelve string guitars [10], the guitar [2] and more in depth for the general case [11]. However, none of these treatments have all of the desired attributes of having a modal basis, uniqueness of the iterative solver solution and provable stability. As this is the case a new formulation is developed here which brings all of these aspects together. The effect of the tension modulation in a string becomes particularly relevant when strings have a low tension (as they tend to on a tanpura) and/or a high Young's modulus and cross sectional radius. The manner in which tension modulation was included will be more discussed in more detail in Section 2.5.

The tanpura's bridge has traditionally been described as a two point bridge, meaning that the string is assumed to terminate at the thread and interacts at only one point on the bridge [12]. A recent paper written by Issanchou et al. [13] demonstrates an impressive agreement between experiments and a time-domain model for a two point bridge system, which is an important step in the validation of models which include non linear contact. This result was found for a high tension of 180.5N and using a guitar string whereas a more common tension for a tanpura string is between 30N and 40N. Hence questions remain regarding as to whether there is a difference between distributed bridge and point bridge interaction at lower tensions and what difference it would make to the jvari. An approach similar to that in [14] here is developed which involves not treating the thread as an end point but as a damper. Following techniques used there the thread and the plucking signal are modelled as single point forces but with a small spatial distribution associated with them. The incorporation of the distributed bridge is outlined in Section 2.7.

## 2. METHOD

### 2.1. Overview

The Newtonian form of the equation which describes the desired system in terms of the string's vertical displacement  $y(x, t)$  (written as  $y$  for brevity), horizontal position  $x$  and time  $t$  can be written

$$\rho A \frac{\partial^2 y}{\partial t^2} = T_0 \frac{\partial^2 y}{\partial x^2} - EI \frac{\partial^4 y}{\partial x^4} - \gamma \frac{\partial y}{\partial t} + \mathcal{F}_{\text{tm}} + \mathcal{F}_c + \mathcal{F}_b + \mathcal{F}_e, \quad (1)$$

where  $\rho$  represents the mass density,  $A$  the cross sectional area,  $E$  the Young's modulus,  $I$  the moment of inertia and  $T_0$  the resting tension of the string.  $\gamma$  gives the effect of frequency dependent damping and will be defined later. The  $\mathcal{F}$  terms on the right-hand side of the equation represent additional force densities which act on the string. Respectively these are due to tension modulation ( $\mathcal{F}_{\text{tm}}$ ), the cotton thread ( $\mathcal{F}_c$ ), the bridge ( $\mathcal{F}_b$ ) and the excitation ( $\mathcal{F}_e$ ). All of these are functions of both  $x$  and  $t$  and are defined over the length of the string ( $L$ ), although some of them only have an effect over a small range of  $x$ . The string is assumed to be simply supported for the boundary conditions.

### 2.2. Modal version

In order to eliminate numerical dispersion a modal framework is used. This involves using the equation

$$y(x, t) = \sum_{i=1}^M v_i(x) \bar{y}_i(t), \quad (2)$$

where  $\bar{y}_i(t)$  are the modal displacements,  $v_i(x) = \sin(\beta_i x)$  are the modal shapes and  $\beta_i = \frac{i\pi}{L}$ . For this to be a perfect representation of the string the number of modes ( $M$ ) would be infinity.

After substituting equation (3) into (1) and integrating spatially over the string the following equation is found which describes the dynamics of a single mode

$$m \frac{\partial^2 \bar{y}_i(t)}{\partial t^2} = -k_i \bar{y}_i(t) - r_i \frac{\partial \bar{y}_i(t)}{\partial t} + \sum_{\epsilon} \bar{F}_{\epsilon, i}(t), \quad (3)$$

where  $m = \frac{\rho AL}{2}$ ,  $k_i = \frac{L}{2}(T_0 \beta_i^2 + EI \beta_i^4)$ ,  $r_i = \frac{L}{2} \gamma(\beta_i)$  and  $\epsilon = \{\text{tm}, \text{c}, \text{b}, \text{e}\}$ .  $\gamma(\beta_i)$  is now expressed as

$$\gamma(\beta_i) = 2\rho A [\sigma_0 + (\sigma_1 + \sigma_3 \beta_i^2) |\beta_i|]. \quad (4)$$

$\sigma_0$ ,  $\sigma_1$  and  $\sigma_3$  shape the frequency dependence to match to a real string as closely as possible [14].  $\bar{F}_{\epsilon, i}$ , the modal driving forces, are derived in different ways according to how the physical effect being considered is modelled. Each one will be explained in its relevant section.

Equation (1) can be rewritten in first-order form, which is exactly equivalent, to read

$$\frac{\partial \bar{y}_i(t)}{\partial t} = \frac{\bar{p}_i(t)}{m} \quad (5)$$

$$\frac{\partial \bar{p}_i(t)}{\partial t} = -k_i \bar{y}_i(t) - r_i \frac{\partial \bar{y}_i(t)}{\partial t} + \sum_{\epsilon} \bar{F}_{\epsilon, i}(t) \quad (6)$$

Where  $\bar{p}_i(t)$  is the momentum equivalent of the  $i^{\text{th}}$  mode.

### 2.3. Single forces of fixed spatial distribution

Some of the force densities will be represented as a single-variable force term which is assumed to be spatially applied to the string according to a fixed distribution function. This is affected by expressing the force densities as the force ( $F_z(t)$ ) multiplied by a spatial distribution function in the following fashion

$$\mathcal{F}_z(x, t) = \psi_z(x) F_z(t), \quad (7)$$

where the spatial distribution  $\psi_z(x)$  is defined as

$$\psi_z(x) = \frac{\pi}{2w_z} \cos \left[ \frac{\pi}{w_z} (x - x_z) \right], \quad (8)$$

inside the domain  $[x_z - \frac{1}{2}w_z, x_z + \frac{1}{2}w_z]$  and 0 otherwise [14].  $w_z$  is the width of the spatial distribution and  $x_z$  the central point. The forces concerned will depend on the averaged string displacement at the point  $x_z$ , which can be written as

$$y_z(t) = \int_{x_z - w_z/2}^{x_z + w_z/2} \psi_z(x) y(x, t) dx \quad (9)$$

Evaluating equation (9) and converting to the modal form, the following equations can be found

$$\bar{F}_{z, i}(t) = g_{z, i} F_z(t), \quad (10)$$

and

$$y_z(t) = \sum_{i=1}^M g_{z, i} \bar{y}_i(t), \quad (11)$$

where

$$g_{z, i} = \frac{\pi^2 \sin(\beta_i x_z) \cos(\frac{\beta_i w_z}{2})}{\pi^2 - \beta_i^2 w_z^2}. \quad (12)$$

### 2.4. Discretisation in time

To solve equations (5) and (6) the following discretisation operators are used to find the system dynamics

$$\delta \phi(t) = \phi^{n+1} - \phi^n \approx \Delta t \frac{\partial \phi(t)}{\partial t} \Big|_{t=(n+\frac{1}{2})\Delta t} \quad (13)$$

$$\mu \phi(t) = \phi^{n+1} + \phi^n \approx 2\phi \Big|_{t=(n+\frac{1}{2})\Delta t}, \quad (14)$$

using  $\Delta t = 1/f_s$ . When discretising equations (5) and (6) it is more compact to use the substitution  $\bar{q}_i^n = \frac{\Delta t}{2m} \bar{p}_i^n$  to give the equations

$$\delta \bar{y}_i^{n+\frac{1}{2}} = \mu \bar{q}_i^{n+\frac{1}{2}} \quad (15)$$

$$\delta \bar{q}_i^{n+\frac{1}{2}} = -a_i \mu \bar{y}_i^{n+\frac{1}{2}} - b_i \delta \bar{y}_i^{n+\frac{1}{2}} + \xi \sum_{\epsilon} \bar{F}_{\epsilon, i}^{n+\frac{1}{2}} \quad (16)$$

at the temporal mid point. The constants are defined as  $\xi = \Delta t^2/(2m)$ ,  $a_i = k_i \Delta t^2/(4m)$  and  $b_i = r_i \Delta t/(2m)$ . The individual cases of  $\bar{F}_{\epsilon, i}^{n+\frac{1}{2}}$  will be explained in their relevant section. To correct for numerical dispersion  $a_i$  and  $b_i$  are replaced by  $a_i^*$  and  $b_i^*$ ; this enforces exact modal frequencies and damping for each mode [14]. The corrected parameters read

$$a_i^* = \frac{1 - 2R_i \Omega_i + R_i^2}{1 + 2R_i \Omega_i + R_i^2} \quad \text{and} \quad b_i^* = \frac{2(1 - R_i^2)}{1 + 2R_i \Omega_i + R_i^2}, \quad (17)$$

where  $R_i = \exp(-\alpha_i \Delta t)$  and  $\Omega_i = \cos(\omega_i \Delta t)$ .

To solve equations (15) and (16) computationally they are rewritten as vectors in the following form:

$$\delta \bar{\mathbf{y}}^{n+\frac{1}{2}} = \mu \bar{\mathbf{q}}^{n+\frac{1}{2}} \quad (18)$$

$$\delta \bar{\mathbf{q}}^{n+\frac{1}{2}} = -\mathbf{A} \mu \bar{\mathbf{y}}^{n+\frac{1}{2}} - \mathbf{B} \delta \bar{\mathbf{y}}^{n+\frac{1}{2}} + \xi \sum_{\epsilon} \bar{\mathbf{F}}_{\epsilon, i}^{n+\frac{1}{2}} \quad (19)$$

In these equations  $A_{ii} = a_i^*$  and  $B_{ii} = b_i^*$  with all off-diagonal elements in both matrices being zero. Using the same procedure taken in previous papers [14] of setting  $\bar{\mathbf{s}} = \delta \bar{\mathbf{y}}^{n+\frac{1}{2}} = \mu \bar{\mathbf{q}}^{n+\frac{1}{2}}$  and then using the relations:

$$\bar{\mathbf{y}}^{n+1} = \bar{\mathbf{s}} + \bar{\mathbf{y}}^n \quad \text{and} \quad \bar{\mathbf{q}}^{n+1} = \bar{\mathbf{s}} - \bar{\mathbf{q}}^n, \quad (20)$$

equation (19) can be re-written as:

$$\mathbf{G} = (\mathbf{I} + \mathbf{A} + \mathbf{B})\bar{\mathbf{s}} - 2(\bar{\mathbf{q}}^n - \mathbf{A}\bar{\mathbf{y}}^n) - \xi \sum_{\epsilon} \bar{\mathbf{F}}_{\epsilon, i}^{n+\frac{1}{2}} = \mathbf{0}, \quad (21)$$

Once the tension modulation, bridge, thread and input modal forces are discretised properly and put into this equation it can be solved iteratively using Newton's method. The Jacobian required for this is

$$\mathbf{J} = \mathbf{J}_s - \xi \sum_{\epsilon} \mathbf{J}_{\epsilon}, \quad (22)$$

where

$$\mathbf{J}_s = \mathbf{I} + \mathbf{A} + \mathbf{B}, \quad (23)$$

and  $\mathbf{J}_{\epsilon}$  are the parts of the Jacobian due to the other forces. All of the parts of the Jacobian will be derived below.

To prevent spectral fold over in the model the number of modes ( $M$ ) must be limited, setting the sizes of  $\bar{\mathbf{y}}$  and  $\bar{\mathbf{q}}$ , so that the frequency of the highest partial is below the Nyquist frequency set by the sampling frequency.

## 2.5. Tension modulation

### 2.5.1. Continuous domain

The force density present in the string due to tension modulation is represented in the following equation

$$\mathcal{F}_{\text{tm}}(x, t) = \frac{EA}{2L} \int_0^L \left( \frac{\partial y}{\partial x} \right)^2 dx \frac{\partial^2 y}{\partial x^2}. \quad (24)$$

Following the procedure for converting to the modal domain this can be rewritten as

$$\mathcal{F}_{\text{tm}}(x, t) = -\frac{EA}{4} \left[ \sum_{i=1}^M \bar{y}_i(t) v_i(x) \beta_i^2 \right] \left[ \sum_{j=1}^M (\beta_j \bar{y}_j(t))^2 \right]. \quad (25)$$

This is found using the orthogonal nature of the sinusoidal basis set within the integral. From this the desired modal force can be derived by multiplying with the modal shape and integrating over the string giving

$$\bar{F}_{\text{tm}, i}(t) = -\Gamma \bar{y}_i(t) \beta_i^2 \left[ \sum_{j=1}^M (\beta_j \bar{y}_j(t))^2 \right], \quad (26)$$

where  $\Gamma = \frac{EAL}{8}$ . This equation shows how the modes are mixed, with tension modulation having the effect of diffusing energy between modes. This is then rewritten in vector form to give:

$$\bar{\mathbf{F}}_{\text{tm}} = -\Gamma (\boldsymbol{\beta}_2 \bar{\mathbf{y}}) \bar{\mathbf{y}}^T \boldsymbol{\beta}_2 \bar{\mathbf{y}}. \quad (27)$$

Where  $\boldsymbol{\beta}_2$  is a diagonal  $M \times M$  matrix with entries along the diagonal of  $\beta_i^2$ .

### 2.5.2. Discretisation of tension modulation equation in time

Equation (27) can be discretised in three ways and equation (28) shows the option that is used. This choice was made as it preserves the uniqueness of the solution to the iterative solver, this will be proven in Section 3.1.

$$\bar{\mathbf{F}}_{\text{tm}}^{n+\frac{1}{2}} = -\frac{\Gamma}{4} (\mu (\bar{\mathbf{y}}^T \boldsymbol{\beta}_2 \bar{\mathbf{y}})) \boldsymbol{\beta}_2 \mu \bar{\mathbf{y}}. \quad (28)$$

After the discretisation operator is applied and using equation (20) the following equation is obtained

$$\bar{\mathbf{F}}_{\text{tm}}(\bar{\mathbf{s}}) = -\frac{\Gamma}{4} ((\bar{\mathbf{y}}^n + \bar{\mathbf{s}})^T \boldsymbol{\beta}_2 (\bar{\mathbf{y}}^n + \bar{\mathbf{s}}) + (\bar{\mathbf{y}}^n)^T \boldsymbol{\beta}_2 \bar{\mathbf{y}}^n) \boldsymbol{\beta}_2 (2\bar{\mathbf{y}}^n + \bar{\mathbf{s}}). \quad (29)$$

This can then be inserted into equation (21). For ease of differentiation (29) is rewritten as

$$\bar{\mathbf{F}}_{\text{tm}}(\bar{\mathbf{s}}) = -\frac{\Gamma}{4} (\alpha_2(\bar{\mathbf{s}}) \mathbf{U}(\bar{\mathbf{s}}) + \alpha_1 \mathbf{U}(\bar{\mathbf{s}})), \quad (30)$$

where

$$\mathbf{U}(\bar{\mathbf{s}}) = \boldsymbol{\beta}_2 (2\bar{\mathbf{y}}^n + \bar{\mathbf{s}}) \quad (31)$$

$$\alpha_2(\bar{\mathbf{s}}) = (\bar{\mathbf{y}}^n + \bar{\mathbf{s}})^T \boldsymbol{\beta}_2 (\bar{\mathbf{y}}^n + \bar{\mathbf{s}}) \quad (32)$$

$$\alpha_1 = (\bar{\mathbf{y}}^n)^T \boldsymbol{\beta}_2 \bar{\mathbf{y}}^n \quad (33)$$

To differentiate  $\alpha_2(\bar{\mathbf{s}})$  with respect to  $\bar{\mathbf{s}}$  the vector calculus rule:

$$\frac{\partial \mathbf{g}(\mathbf{x})^T \mathbf{C} \mathbf{h}(\mathbf{x})}{\partial \mathbf{x}} = \mathbf{g}(\mathbf{x})^T \mathbf{C} \frac{\partial \mathbf{h}(\mathbf{x})}{\partial \mathbf{x}} + \mathbf{h}(\mathbf{x})^T \mathbf{C}^T \frac{\partial \mathbf{g}(\mathbf{x})}{\partial \mathbf{x}}, \quad (34)$$

is used. In the equation being considered  $\boldsymbol{\beta}_2$  which corresponds to  $\mathbf{C}$  is diagonal so it is equal to its own transpose. This gives:

$$\frac{\partial \alpha_2(\bar{\mathbf{s}})}{\partial \mathbf{x}} = 2(\bar{\mathbf{s}} + \bar{\mathbf{y}}^n)^T \boldsymbol{\beta}_2. \quad (35)$$

Differentiating  $\mathbf{U}(\bar{\mathbf{s}})$  with respect to  $\bar{\mathbf{s}}$  gives

$$\frac{\partial \mathbf{U}(\bar{\mathbf{s}})}{\partial \bar{\mathbf{s}}} = \boldsymbol{\beta}_2. \quad (36)$$

Then using the product rule the Jacobian of the tension modulation part of the  $\mathbf{G}$  function can be written as

$$\mathbf{J}_{\text{tm}}(\bar{\mathbf{s}}) = -\frac{\Gamma}{4} (\alpha_2 \boldsymbol{\beta}_2 + \mathbf{U}(\bar{\mathbf{s}}) (2(\bar{\mathbf{s}} + 2\bar{\mathbf{y}}^n)^T \boldsymbol{\beta}_2) + \alpha_1 \boldsymbol{\beta}_2). \quad (37)$$

As  $\mathbf{J}_{\text{tm}}$  is a full matrix the addition of the tension modulation significantly increases computational time due to the linear system solving required in each iteration.

It has been shown by Bilbao [8] that, using a similar modal formulation, significant pitch glide in the wrong direction can arise due to tension modulation if the number of modes used creates partials up to the Nyquist frequency. However it was found that this spurious effect could not be replicated in the model even for extreme amplitudes.

## 2.6. Thread

### 2.6.1. Continuous domain

In the model the thread is treated as described in Section 2.3. The equation for the force is

$$F_c(t) = K_c(h_c - y_c(t)) - R_c \frac{\partial y_c(t)}{\partial t}, \quad (38)$$

where  $K_c$  is the spring stiffness of the thread,  $y_c$  is the vertical displacement of the string at the thread point,  $t$  is the time,  $h_c$  is the thread equilibrium point and  $R_c$  is the thread loss parameter.  $h_c$  was set to zero for all modelling purposes and as such will be omitted in the following equations. When re-expressed in the modal domain this equation reads

$$\bar{F}_{c,i}(t) = -g_{c,i} \sum_{i=1}^M g_{c,i} \left( K_c \bar{y}_i(t) + R_c \frac{\partial \bar{y}_i(t)}{\partial t} \right). \quad (39)$$

### 2.6.2. Discretisation of thread equation in time

Using the discretisation operators on the force function and the equation  $\bar{y}_i^{n+1} = \bar{s}_i + \bar{y}_i^n$  the equation for the modal force at time step  $n + \frac{1}{2}$  can be written

$$\bar{\mathbf{F}}_c^{n+\frac{1}{2}} = -\mathbf{g}_c \mathbf{g}_c^\top \left( \frac{K_c}{2} (\bar{\mathbf{s}} + 2\bar{\mathbf{y}}^n) + \frac{R_c}{\Delta t} \bar{\mathbf{s}} \right), \quad (40)$$

in vector form. To solve for  $\bar{\mathbf{s}}$  the Jacobian of this vector is required. This is:

$$\mathbf{J}_c = -\left( \frac{K_c}{2} + \frac{R_c}{\Delta t} \right) \mathbf{g}_c \mathbf{g}_c^\top. \quad (41)$$

## 2.7. Distributed Barrier

### 2.7.1. Continuous domain and spatial discretisation

To model the bridge a contact law is used to simulate the compression of the string and barrier. The contact law used is

$$\mathcal{F}_b(x, t) = k_b [h_b(x) - y(x, t)]^\alpha, \quad (42)$$

where  $k_b$  is the barrier stiffness per unit length,  $h_b(x)$  is the height of the bridge at position  $x$  and  $\alpha$  is the exponent that governs the bridge interaction. Following [14] the exponent is set according to Hertzian theory as  $\alpha = 1$  and the formulation is carried out with this in place. Other choices of  $\alpha \geq 1$  are possible and all of the terms required for solving related to the bridge can be derived in this general case. The force density and the string displacement in this equation are defined over  $[x_b - \frac{1}{2}\omega_b, x_b + \frac{1}{2}\omega_b]$  which is the spatial domain of the bridge; the force density will be zero outside this region. The potential energy density for the bridge will also be required

$$\mathcal{V}_b(x, t) = \frac{k_b}{2} [h_b(x) - y(x_b, t)]^2, \quad (43)$$

as will another definition for the force

$$\mathcal{F}_b(x, t) = -\frac{\partial \mathcal{V}_b}{\partial y}. \quad (44)$$

For use in equation (21) the modal force vector  $\bar{\mathbf{F}}_b$  must be found. This would usually be done by integrating over the length of the string as follows

$$\bar{F}_{b,i}(t) = \int_0^L v_i(x) \mathcal{F}_b(x, t) dx, \quad (45)$$

but due to the non-analytic nature of  $\mathcal{F}_b(x, t)$  it is approximated as a Riemann sum [9]

$$\bar{F}_{b,i}(x, t) \approx \sum_{k=1}^K v_{i,k} \mathcal{F}_{b,k}(x_k, t) \Delta x. \quad (46)$$

The bridge is defined to have  $K$  points along its length,  $v_{i,k}$  gives each modal amplitude at the spatial position  $k$  in the domain of the barrier and  $\mathcal{F}_{b,k}(x_k, t)$  is the contact force density at point  $k$  and time  $t$ .

### 2.7.2. Discretisation of bridge equation in time

Writing the potential density at time step  $n$  gives

$$\mathcal{V}_{b,k}^n(t) = \frac{k_b}{2} [h_{b,k} - y_k^n]^2, \quad (47)$$

here  $y_k^n$  is at the corresponding bridge point to  $h_{b,k}$  in each case. Equation (44) is discretised in time to give

$$\mathcal{F}_{b,k}^{n+\frac{1}{2}} = -\frac{\mathcal{V}_{b,k}^{n+1} - \mathcal{V}_{b,k}^n}{y_k^{n+1} - y_k^n}. \quad (48)$$

These equations are combined to give

$$\mathcal{F}_{b,k}^{n+\frac{1}{2}} = -\frac{k_b}{2} \frac{[h_{b,k} - (s_k + y_k^n)]^2 - [h_{b,k} - y_k^n]^2}{s_k}. \quad (49)$$

Where again  $s_k$  is at the corresponding barrier point to  $h_{b,k}$ . Following from equation (49) and vectorising gives the equation

$$\bar{\mathbf{F}}_b^{n+\frac{1}{2}} = \Delta x \mathbf{V}^\top \mathcal{F}_b^{n+\frac{1}{2}}, \quad (50)$$

where  $\mathbf{V}$  is a  $K \times M$  matrix which holds all of the modal shapes at each point along the bridge.  $\bar{\mathbf{F}}_b^{n+\frac{1}{2}}$  must be differentiated with respect to  $\bar{\mathbf{s}}$  for use in Newton's method so this is done by using the chain rule, giving the Jacobian for the barrier as

$$\mathbf{J}_b = \Delta x \mathbf{V}^\top \frac{\partial \mathcal{F}_b^{n+\frac{1}{2}}}{\partial \mathbf{s}} \frac{\partial \mathbf{s}}{\partial \bar{\mathbf{s}}}, \quad (51)$$

where

$$\mathbf{y} = \mathbf{V} \bar{\mathbf{y}} \quad \text{and} \quad \mathbf{s} = \mathbf{V} \bar{\mathbf{s}}. \quad (52)$$

Obviously  $\frac{\partial \mathbf{s}}{\partial \bar{\mathbf{s}}} = \mathbf{V}$ . Explicitly  $\mathbf{J}_b$  is written as

$$\mathbf{J}_b = \frac{k_b \Delta x}{2} \mathbf{V}^\top \boldsymbol{\zeta} \mathbf{V}, \quad (53)$$

where  $\boldsymbol{\zeta}$  is a diagonal matrix with the dimensions  $K \times K$ . The diagonal entries in the matrix range from  $\zeta_{1,1}$  which is the closest bridge point to the thread to  $\zeta_{K,K}$  which is the furthest bridge point from the thread are:

$$\zeta_{k,k} = \frac{[h_{b,k} - (s_k + y_k^n)]^2 - [h_{b,k} - y_k^n]^2}{s_k^2} - \frac{2[h_{b,k} - (s_k + y_k^n)]}{s_k}. \quad (54)$$

### 2.7.3. Single point bridge

For comparison the distributed bridge was made replaceable by a single point bridge in the model. The single force bridge has a different equation for the force density which is

$$\mathcal{F}_b(x, t) = \delta(x - x_b) k_b [h_b(x) - y(x, t)], \quad (55)$$

$x_b$  here is the spatial position of the bridge point. When this is put into equation (45) the integral becomes exactly solvable and gives a modal force for mode  $i$  of

$$\bar{F}_{b,i}(t) = v_i(x_b) k_b [h_b(x_b) - y(x_b, t)]. \quad (56)$$

## 2.8. Plucking signal

The plucking signal used is a single point force spatially distributed following the procedure outlined in Section 2.3. The input force used [14] is

$$F_e(t) = A_e \sin^2 \left( \frac{\pi}{\tau_e} h_e(t - t_e) \right), \quad (57)$$

where

$$h_e(t) = \frac{1}{2} \cos \left( t + \frac{\tau_e \sinh(\Omega t) / \tau_e}{\sinh(\Omega t)} \right). \quad (58)$$

$F_e(t)$  is zero outside of the time domain  $t_e : t_e + \tau_e$  where  $t_e$  is the excitation time and  $\tau_e$  is the length of the excitation. This gives a malleable curve based on  $\sin^2$  whose central point and gradients on either side can be altered according to the choice of  $\Omega$ . This is to a certain extent an arbitrary choice and was chosen to simulate the plucking typically used in the playing of tanpura.

As  $F_e$  is known at all time steps it can simply be inserted into equation (21) by using the modal weight  $\mathbf{g}_e$  and discretisation operator  $\mu$

$$\bar{\mathbf{F}}_e^{n+\frac{1}{2}} = \frac{1}{2} \mathbf{g}_e \mu F_e. \quad (59)$$

## 3. MODEL PROPERTIES

### 3.1. Uniqueness

For the scheme to have a unique existent solution the Jacobian must be positive definite. In this scheme the Jacobian is equation (22). For a  $N \times N$  symmetric matrix ( $\mathbf{M}$ ) to be positive definite it is required that

$$\mathbf{z}^\top \mathbf{M} \mathbf{z} > 0, \quad (60)$$

for all real column vectors  $\mathbf{z}$  of size  $N$  which are non-zero. It is useful in this instance to note that the addition of a positive semi-definite matrix to a positive definite matrix results in a matrix which is still positive definite. The definition for a positive semi-definite matrix being

$$\mathbf{z}^\top \mathbf{M} \mathbf{z} \geq 0, \quad (61)$$

$\mathbf{J}_s$  is positive definite as every matrix in it has only real, positive entries and they are all diagonal. For the thread term  $-\mathbf{J}_c$  can be proven to be positive semi definite simply by considering that any negatives in either  $\mathbf{z}$  or  $\mathbf{g}_c$  are squared in equation (62), proving that

$$\mathbf{z}^\top \mathbf{g}_c \mathbf{g}_c^\top \mathbf{z} \geq 0, \quad (62)$$

The term  $-\zeta$  is positive semi-definite as  $-\zeta_{k,k}$  is a convex function [5] of  $\bar{\mathbf{s}}$  which means that  $-\mathbf{J}_b$  is also positive semi-definite due to the following relation

$$-\mathbf{z}^\top \mathbf{J}_b \mathbf{z} = -\frac{\Delta x k_b}{2} (\mathbf{V}^\top \mathbf{z})^\top \zeta^n (\mathbf{V}^\top \mathbf{z}) \geq 0. \quad (63)$$

To prove that  $-\mathbf{J}_{tm}$  is positive semi-definite it is easiest to consider it in its three parts as seen in equation (37).  $\alpha_2$ ,  $\alpha_1$  and  $\Gamma$  are all positive and  $\beta_2$  is a diagonal matrix with only positive entries. Following from this the following must be true for the first and third matrices on the right hand side of equation (37)

$$\mathbf{z}^\top \alpha_2 \Gamma \beta_2 \mathbf{z} \geq 0 \quad \text{and} \quad \mathbf{z}^\top \alpha_1 \Gamma \beta_2 \mathbf{z} \geq 0. \quad (64)$$

Expanding the remaining matrix and using  $\beta_2^\top = \beta_2$  where appropriate and writing  $\lambda = \bar{\mathbf{s}} + 2\bar{\mathbf{y}}^n$

$$\mathbf{U}(\bar{\mathbf{s}}) (2\lambda^\top \beta_2) = 2\beta_2 \lambda \lambda^\top \beta_2^\top. \quad (65)$$

After rearranging it can be seen that the following must be true.

$$2\Gamma \mathbf{z}^\top \beta_2 \lambda \lambda^\top \beta_2^\top \mathbf{z} \geq 0 \quad (66)$$

Therefore  $-\mathbf{J}_{tm}$  is positive semi-definite. As all of the component matrices of  $\mathbf{J}$  are positive definite or positive semi-definite the uniqueness of the solution is proven.

### 3.2. Stability

The total numerical energy of the system at time-step  $n$  can be expressed as a summation of the total energies of the modes of the stiff string with the potentials due to the tension modulation, thread and barrier added on. The potential due to the barrier at time step  $n$  can be easily found using equation (47)

$$V_b^n = \Delta x (\mathbf{1}_K)^\top \mathbf{V}_b^n. \quad (67)$$

Where  $\mathbf{1}_K$  is a vector of size  $K$  with 1 at every entry. The potential due to the tension modulation is

$$V_{tm}^n = \frac{\Gamma}{4} ((\bar{\mathbf{y}}^n)^\top \beta_2 \bar{\mathbf{y}}^n)^2, \quad (68)$$

and the potential due to the thread is

$$V_c^n = \frac{K_c}{2} (\mathbf{g}_c^\top \bar{\mathbf{y}}^n)^2, \quad (69)$$

which in conjunction with the energy

$$H_s^n = \xi^{-1} ((\bar{\mathbf{y}}^n)^\top \mathbf{A} \bar{\mathbf{y}}^n + (\bar{\mathbf{q}}^n)^\top \bar{\mathbf{q}}^n), \quad (70)$$

give the total numerical energy at time-step  $n$

$$H^n = V_b^n + V_{tm}^n + V_c^n + H_s^n. \quad (71)$$

To get a power balance the right hand side of equation (19) is multiplied by  $(\delta \bar{\mathbf{y}}^n)^\top$  and the left hand side by  $(\mu \bar{\mathbf{q}}^n)^\top$ . Following various re-arrangements the equation for the energy balance is found to be

$$\Delta t^{-1} \delta H^{n+\frac{1}{2}} = P^{n+\frac{1}{2}} - Q^{n+\frac{1}{2}}. \quad (72)$$

The input power  $P^{n+\frac{1}{2}}$  is

$$P^{n+\frac{1}{2}} = \frac{1}{2\Delta t} \mathbf{g}_c^\top \delta \bar{\mathbf{y}}^{n+\frac{1}{2}} \mu F_e^{n+\frac{1}{2}}, \quad (73)$$

and the power losses  $Q^{n+\frac{1}{2}}$  are

$$Q^{n+\frac{1}{2}} = \frac{(\delta \bar{\mathbf{y}}^{n+\frac{1}{2}})^\top \mathbf{B} \delta \bar{\mathbf{y}}^{n+\frac{1}{2}}}{\xi \Delta t} + \frac{R_c}{\Delta t^2} (\delta y_c^{n+\frac{1}{2}})^2. \quad (74)$$

As both  $\mathbf{A}$  and  $\mathbf{B}$  are positive definite  $H^{n+\frac{1}{2}}$  and  $Q^{n+\frac{1}{2}}$  can only be greater than or equal to zero so the change in the numerical energy of the system can only be conserved or decline outwith periods where energy is being directed into the system via the controlled input force.

String Parameters			
	C <sub>3</sub>	C <sub>2</sub>	unit
$L$	1.0	1.0	m
$\rho$	7850	8000	kg/m <sup>3</sup>
$A$	$6.16 \times 10^{-8}$	$2.83 \times 10^{-7}$	m <sup>2</sup>
$E$	$2.0 \times 10^{11}$	$1.0 \times 10^{11}$	N/m <sup>2</sup>
$I$	$3.02 \times 10^{-16}$	$6.36 \times 10^{-15}$	kg/m <sup>2</sup>
$T_0$	33.1	38.7	N
$\sigma_0$	0.6	0.8	s <sup>-1</sup>
$\sigma_1$	$6.5 \times 10^{-3}$	$6.5 \times 10^{-3}$	m/s
$\sigma_3$	$5 \times 10^{-6}$	$5 \times 10^{-6}$	m <sup>3</sup> /s

 Table 1: Physical parameter values used for C<sub>3</sub> and C<sub>2</sub> string.

## 4. RESULTS

### 4.1. String and contact parameters

The string parameters used in the model are detailed in Table 1. Parameters chosen to represent a steel C<sub>3</sub> string were the same as used in previous papers studying the tanpura [14]. For modelling a bronze C<sub>2</sub> string the values for  $\sigma_1$  and  $\sigma_3$  were set to be the same as for the steel string for convenience whilst the value for  $\sigma_0$  was altered to get an empirically more realistic response.

The bridge profile was taken to be

$$h_b(x) = 3(x - x_b)^2, \quad (75)$$

which is based upon measurements taken by Guettler [15].  $x_b$  is the central point of the barrier. For the spring stiffness of the barrier a value of  $k_b = 1 \times 10^{11}$  N/m<sup>2</sup> was used. The width was chosen to be wide enough such that the end points of the barrier were not touched during vibration. This limits the string's interaction with the bridge to be within the space in which the bridge is defined. The position of the bridge maximum was set to be 10 mm while the bridge width required was found to be 1 mm for the C<sub>3</sub> and 1.5 mm for the C<sub>2</sub>. The number of points was altered from being very high, around 60, down to 11 for C<sub>3</sub> and 16 for C<sub>2</sub>. The smaller numbers gave almost exactly the same results as were found when 60 bridge points were used.  $K_c$  was chosen to be  $1.2 \times 10^5$  N/m and  $R_c$  was taken to be 1.2 kg/s [14]. The thread position was set to 5 mm when modelling the C<sub>3</sub> string and 4 mm when modelling the C<sub>2</sub> string.

The plucking parameters used to generate results were  $x_e = 0.37 \times L$  m,  $w_e = 1.5$  mm,  $A_e = -0.5$  N,  $\Omega = 30$ ,  $\tau_e = 0.01$  s and  $t_e = 0$  s.

### 4.2. Convergence

The top row of graphs in Figure 2 shows the nut force over time with different sampling frequencies. It can be seen that the envelope shapes are very similar between the two cases with only small variations in the detail. The close match between the envelopes shows that the model does a good job of replicating global trends at lower sampling frequencies.

The second row of graphs shows the nut force over two different time frames, one very soon after the string is plucked and the other roughly 0.15 s after. The higher sampling rate plots which are the red and dashed black lines match up well over both plots. The lower sampling frequency causes the plot to be compressed

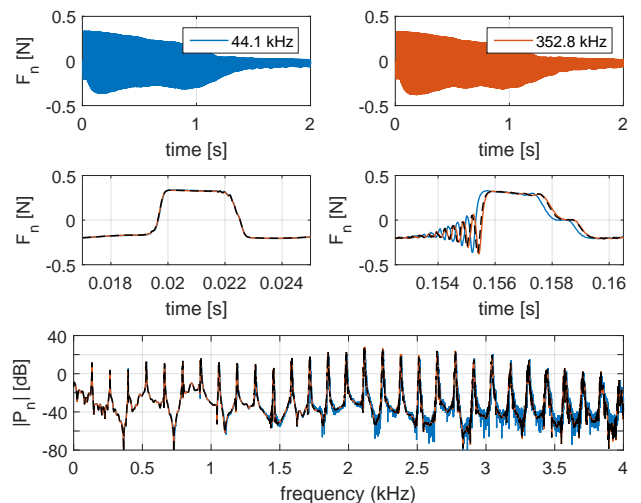


Figure 2: Plots showing how the sampling frequency affects the output from the model. The top two graphs show the nut force over time for two sampling frequencies. The middle plots display short portions of the nut force signal over a short time frame. These can be compared to the black dashed line which represents  $F_s = 352.8$  kHz but the number of modes is truncated to be the same as the number of modes in the  $F_s = 44.1$  kHz case. The final plot shows the radiated pressure due to the nut force over a range of frequencies with the same colour scheme as the other graphs.

along the time axis which is what is shown in the later time snapshot. This is due to the numerical model with lower sampling rates effecting a reduced contact stiffness leading to increased contact durations. The shape of the signal is preserved however, meaning that general phenomena within the signal will be captured. This does however mean that for any comparison to experiment high sampling rates are required to get the signals to match up well over time. This was noted by Issanchou et al [13] when performing their comparison between experiment and simulation. While the black dashed line and the red line are signals generated at the same sampling frequency the number of modes used when generating the black dashed line were restricted to be the same as the number used in generating the blue signal. It is clear from these plots that including modes above the audio band has little effect on the area of interest. Hence these modes could, in the future, be ignored speeding up computation times significantly.

The final graph in Figure 2 shows the spectral envelope of the radiated nut pressure signal over a range of frequencies. Again it can be seen that there is a strong agreement between all of the lines. The differences are at such a low pressure level that they are perceptually insignificant, as are the small discrepancies in the partial frequencies. Indeed, informal listening test indicated that the three signals are aurally barely distinguishable.

### 4.3. Tanpura simulation

When analysing the information generated by the model the most important data is that which pertains to how the signal generated would sound. To investigate this the nut force is computed and is filtered by a body response measured with an impact hammer by a microphone 80 cm away [14]. This allows a physically meaningful

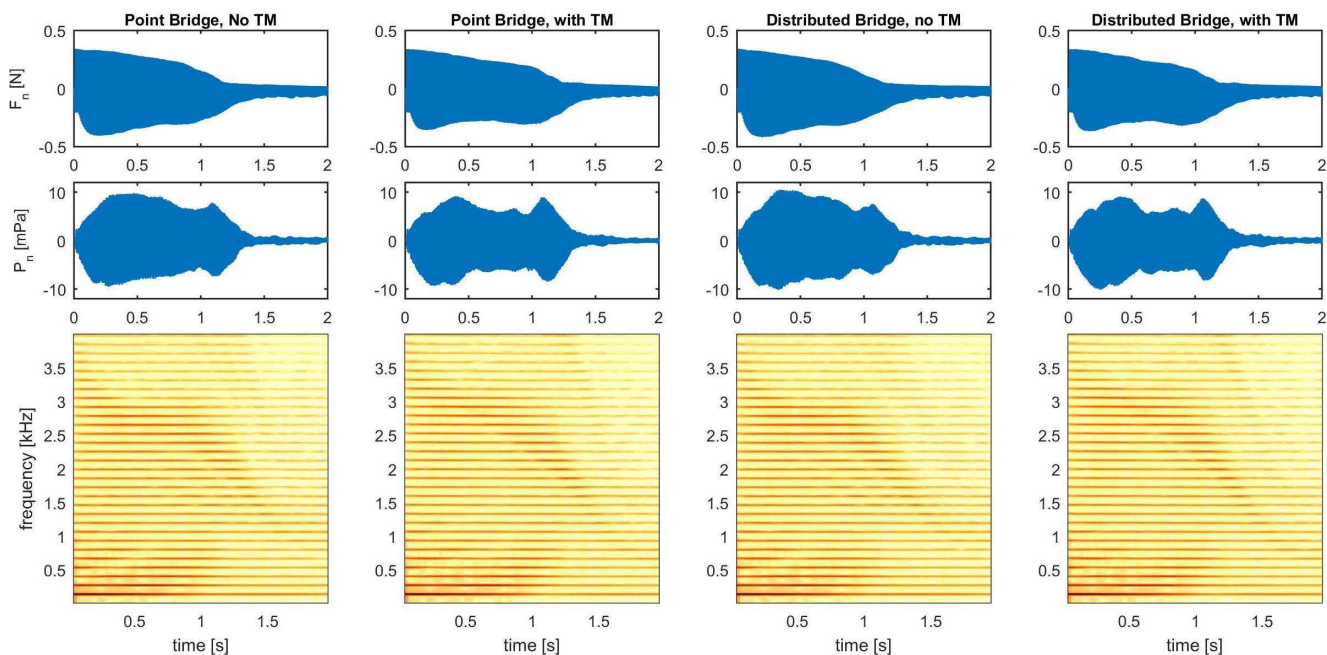


Figure 3: Plots showing two seconds of simulation after the start of the pluck. The top row shows the nut force envelope over time for the four cases indicated by the note on top of the graph. The second row shows the radiated pressure from the nut envelope over time. The third row shows spectrograms of the nut force.

signal to be generated from the model which when analysed will give information on how the changes being investigated will affect the perceived sound from the modelled instrument.

Figure 3 shows the nut force, radiation pressure from the nut force and spectrograms for the four different configurations of including tension modulation and having a point or distributed bridge. These were all set up with the same parameter values (barring the changes made to investigate) and identical plucking conditions. The simplest case presented here with no tension modulation and a point bridge is used as a point of comparison when studying the effects of adding tension modulation and a distributed barrier. Within the spectrograms the *jvari* is the time-dependent formant of pronounced frequencies which have the drop in spectral centroid followed by a plateau followed again by a drop. As can be seen from Figure 3 all of the spectrograms show this behaviour, however there are differences in the characteristics of the *jvari* shapes.

In the radiated pressure time-domain graph the tension modulation can be seen to significantly alter the envelope in the first half second of the simulation and the loss of energy at the end of the signal also follows a different shape. From the spectrograms it can be observed that the addition of tension modulation causes the spectral centroid of the *jvari* to start at a higher frequency and the plateau is also at a higher frequency relative to the situation without the tension modulation. The effect on the tail of the *jvari* is hard to see in the spectrograms. The tension modulation also has the expected effect of causing pitch glide in the partials. This can be seen by zooming in on the partials above 3 kHz in the second and fourth spectrograms.

Distribution of the bridge forces has the effect of shortening the plateau of the *jvari* when compared to the point barrier and it also rounds off the top right corner of the plateau. This effect can be seen in both the spectrogram and the radiated pressure plot. The

start of the tail can be seen to occur at roughly 1 second when the barrier is distributed and roughly 0.1 s later with the point barrier. Although they start to decay at different times they end up with a very similar level of energy left in the system.

When the tension modulation and distributed bridge are combined the spectrogram is distinct from all three of the others, indicating that both additions make a difference to the output of the model. This spectrogram shows the higher starting point frequency and plateau frequency for the *jvari* from the tension modulation and the more rounded, shorter plateau from the distributed barrier. The extra effect of having both together is difficult to see in plots, but when listening to sound examples<sup>1</sup> the combination appears to give a "livelier" sound than any of the signals generated by the other model options.

The effect due to the tension modulation can be seen more clearly in Figure 4. The plots show spectrograms of the nut force when the model is run with  $C_2$  string parameters and a greater excitation amplitude of  $A_e = -0.8$  N. It can be observed by comparing (a) and (b) to (c) and (d) that the tension modulation is noticeable when the barrier is absent but has a larger effect when the barrier is present. With these parameters the change in the shape of the *jvari* is more significant than in the  $C_3$  case and is heard more clearly in sound examples.

## 5. CONCLUSIONS

This paper shows how tension modulation, a distributed barrier and the thread can be included in a model of the tanpura. The model is proven to be unconditionally stable and to have a unique solution to the non-linear vector equation that has to be solved at

<sup>1</sup><http://www.socasites.qub.ac.uk/mvanwalstijn/dafx17c/>

## 6. REFERENCES

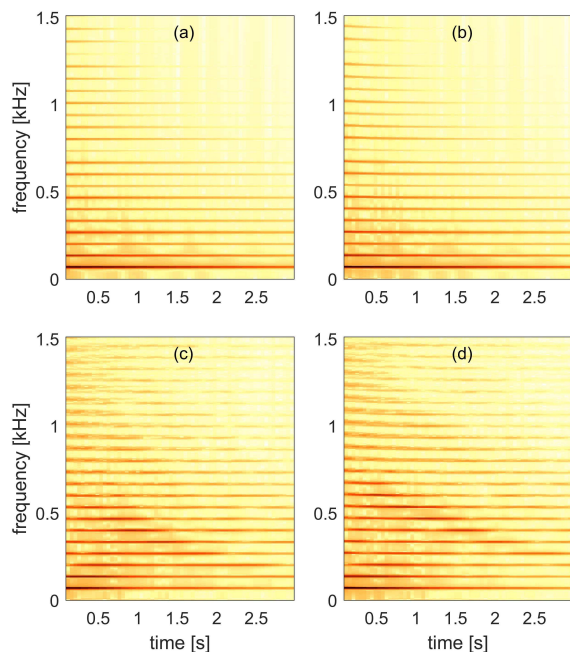


Figure 4: Spectrograms of the nut force for four configurations comparing the effects of tension modulation with and without tension modulation. *a* has no bridge or tension modulation, *b* has no bridge but with tension modulation, *c* has a bridge but with no tension modulation and *d* has both the bridge and tension modulation.

each time step. The results discussed show that both tension modulation and a distributed bridge have small effects on the shape of the jvari. A webpage<sup>2</sup> has been created with sound clips corresponding to each of the signals presented in Figures 3 and 4. These sound clips provide a way to interpret the results in a manner more natural to the study of the sound produced by a tanpura. It is worth noting that this model is not suitable for use in real time applications without dedicated hardware as 1 s of simulation at 44.1 kHz takes 81 s without tension modulation and 131 s with tension modulation.

The model presented here could be expanded further by including a transverse plane of oscillation in a similar way to other models detailed in the past [13, 3]. Coupling at termination points between transverse planes of oscillation and including friction as the string moves across the barrier has been found to make a difference to the jvari in simulations [16] and experimental investigation into the physical extent of these effects is another avenue that could be explored. Tension modulation in the two plane case will be important as it provides coupling when there is a phase difference between the oscillations in the two planes. A more quantitative method of comparing the spectrograms of signals would be useful in making comparisons between cases easier.

<sup>2</sup><http://www.socasites.qub.ac.uk/mvanwalstijn/dafx17c/>

- [1] C. V. Raman, “On some Indian stringed instruments,” *Proc. Indian Assoc. Cultiv. Sci.*, vol. 7, pp. 29–33, 1921.
- [2] S. Bilbao and A. Torin, “Numerical Simulation of String/Barrier Collisions: The Fretboard,” in *DAFx*, 2014, pp. 137–144.
- [3] C. Desvages and S. Bilbao, “Two-Polarisation Physical Model of Bowed Strings with Nonlinear Contact and Friction Forces, and Application to Gesture-Based Sound Synthesis,” *Applied Sciences*, vol. 6, no. 5, pp. 135, May 2016.
- [4] V. Chatziioannou and M. Van Walstijn, “An energy conserving finite difference scheme for simulation of collisions,” in *Proc. Stockholm Musical Acoust. Conf*, 2013.
- [5] V. Chatziioannou and M. van Walstijn, “Energy conserving schemes for the simulation of musical instrument contact dynamics,” *Journal of Sound and Vibration*, vol. 339, pp. 262–279, Mar. 2015.
- [6] Stefan Bilbao, Alberto Torin, and Vasileios Chatziioannou, “Numerical modeling of collisions in musical instruments,” *Acta Acustica united with Acustica*, vol. 101, no. 1, pp. 155–173, 2015.
- [7] S. Bilbao, “Numerical Modeling of String/Barrier Collisions,” in *Proc. ISMA*, 2014, pp. 267–272.
- [8] S. Bilbao, *Numerical Sound Synthesis*, Wiley & Sons, Chichester, UK, 2009.
- [9] M. van Walstijn and J. Bridges, “Simulation of distributed contact in string instruments: A modal expansion approach,” Aug. 2016, pp. 1023–1027, IEEE.
- [10] V. Debut, J. Antunes, M. Marques, and M. Carvalho, “Physics-based modeling techniques of a twelve-string Portuguese guitar: A non-linear time-domain computational approach for the multiple-strings/bridge/soundboard coupled dynamics,” *Applied Acoustics*, vol. 108, pp. 3–18, July 2016.
- [11] M. Ducceschi, S. Bilbao, and C. Desvages, “Modelling collisions of nonlinear strings against rigid barriers: Conservative finite difference schemes with application to sound synthesis,” in *Proc. International Congress on Acoustics*, Sept. 2016.
- [12] C. Valette, C. Cuesta, M. Castellengo, and C. Besnainou, “The tampura bridge as a precursive wave generator,” *Acta Acustica united with Acustica*, vol. 74, no. 3, pp. 201–208, 1991.
- [13] C. Issanchou, S. Bilbao, J.L. Le Carrou, C. Touze, and O. Doare, “A modal-based approach to the nonlinear vibration of strings against a unilateral obstacle: Simulations and experiments in the pointwise case,” *Journal of Sound and Vibration*, vol. 393, pp. 229–251, Apr. 2017.
- [14] M. van Walstijn, J. Bridges, and S. Mehes, “A real-time synthesis oriented tanpura model,” in *Proc. Int. Conf. Digital Audio Effects (DAFx-16)*, 2016.
- [15] K. Guettler, “On the string-bridge interaction in instruments with a one-sided (bridge) constraint,” available from *knutsacoustics.com*, 2006.
- [16] J. Bridges and M. Van Walstijn, “Investigation of tanpura string vibrations using a two-dimensional time-domain model incorporating coupling and bridge friction,” *Proc. of the third Vienna Talk on Music Acoustics*, 2015.